Pergamon

0301-9322(95)00020-8

Int. J. Multiphase Flow Vol. 21, No. 6, pp. 1003–1024, 1995

0301-9322/95 $9.50 + 0.00

LOCAL HEAT TRANSFER COEFFICIENTS ON THE CIRCUMFERENCE OF A TUBE IN A GAS FLUIDIZED BED

SURESH R. SUNDERESAN and NIGEL N. CLARK

Department of Mechanical and Aerospace Engineering, West Virginia University, Morgantown, WV 26506-6106, U.S.A.

(Received 18 June 1994; in revised form 27 February 1995)

Abstract—A heated horizontal heat transfer tube was installed 14.8 cm above the distributor plate in a square fluid bed measuring 30.5 × 30.5 cm. Four different Geldart B sized particle beds were used (sand of two different distributions, an abrasive and glass beads) and the bed was fluidized with cold air. The tube was instrumented with surface thermocouples around half of the tube circumference and with differential pressure ports that can be used to infer bubble presence. Numerical execution of the transient conduction equation for the tube allowed the local time-varying heat transfer coefficient to be extracted. Data confirm the presence of the stagnant zone on top of the tube associated with low superficial velocities. Auto-correlation of thermocouple data revealed bubble frequencies and the cross-correlation of thermal and pressure events confirmed the relationship between the bubbles and the heat transfer events. In keeping with the notion of a "Packet renewal" heat transfer model, the average heat transfer coefficient was found to vary in sympathy with the root-mean square amplitude of the transient heat transfer coefficient.

Key words: fluidized bed, heat transfer, instrumentation, bubbles

1. INTRODUCTION

Fluidized beds are widely used in a variety of industries, for example in chemical reactors and regeneration processes, where the heat transfer properties of the fluidized system become important for successful operation. The heat transfer in the bed is achieved by contact of the bed particles with an appropriate heat exchanger surface, often an in-bed tube or a water-wall. The study of bed-to-surface heat transfer coefficients is needed in order to design the fluidized bed for physical and chemical operations, where the control of temperature plays an important role. Research has been undertaken by many previous workers in an effort to understand the mechanism of the heat transfer but the knowledge of transient contact between the bed emulsion and the local tube surface is still inadequate. Measurement of the time-varying temperatures of the immersed surface in the bed and subsequent calculation of the local time-varying surface heat transfer coefficients provides a method for pursuing a better understanding of the local transient behavior of the heat transfer tube since it has previously been observed that the contact characteristics were different at various angular positions around the immersed surface (tube). Such transient measurements are of interest in modeling the passing voids for the case of bubbling beds and may ultimately lead to better selection and positioning of the heat exchanger tubes for use in bubbling beds.

2. LITERATURE REVIEW AND BACKGROUND

The local instantaneous heat transfer coefficient $h_i(t)$ at any time t and at any point on the surface can be written as,

$$q_i''(t) = h_i(t)[T_{wall}(t) - T_{bed}] \quad [1]$$

where, $q_i''(t)$ is the instantaneous local surface heat flux, $h_i(t)$ is the local instantaneous heat transfer coefficient, $T_{wall}(t)$ is the instantaneous local wall (surface) temperature and T_{bed} is the near-constant bulk temperature of the bed. To calculate the local instantaneous heat transfer coefficient from [1], it is necessary to have the local instantaneous heat flux at the surface, the time-varying surface

temperature and the bulk temperature of the bed. The bed bulk temperature is considered to remain constant at a measured value, which reduces the required transient measurements to local instantaneous surface temperature and heat flux.

George (1987) used a heat flux transducer to measure the local instantaneous heat transfer from an immersed surface to a high temperature fluidized bed. The transducer body was made of 304 stainless steel that incorporated two eroding type thermocouple junctions. The junction was formed by small burrs at the surface that bridged over thin mica sheets that separated thermocouple metals which were isolated from transducer body. The transducer was embedded in the surface and measured transient surface temperatures over a period of time. The small burrs that formed the junction renewed themselves as the surface was slowly eroded by the fluidized bed. Unidirectional unsteady heat transfer was assumed to occur within the transducer between the surface and the in-wall thermocouples. The surface temperature fluctuations were so rapid that they were damped out before penetrating the thickness of the surface so that the conduction problem was considered to be semi-infinite with a constant in-wall temperature. Instantaneous surface heat flux was solved as the sum of a time-average heat flux and a function of time representing fluctuations of the heat flux. The solution was obtained mathematically for a step change in the surface temperature. George & Smalley (1991) used a heat flux transducer with analog signal conditioning equipment to measure the instantaneous local heat transfer rates to an immersed horizontal cylinder. The mounting arrangement allowed the cylinder to rotate to different angular positions and the single heat flux transducer was used to take the data at different angular positions. George (1993) conducted another study by using the heat flux transducer used by George & Smalley (1991) to measure the instantaneous heat fluxes on the immersed surface in the bed. The author showed that the instrumentation for measuring the fluctuations on the heat transfer surface should be designed for a minimum bandwidth of 100 Hz to identify the local maxima and minima of the instantaneous heat transfer coefficients. The signal conditioning circuit used in George's study provided an output voltage that was linearly related to the instantaneous heat flux on the surface.

Khan & Turton (1992) developed a method to measure local instantaneous heat fluxes simultaneously with three surface mounted transducers separated at an angle of 120° in the wall of a 50 mm outer diameter stainless steel cylindrical heat transfer tube. The inner diameter of the heat transfer tube was 25 mm. The tube was placed in a hot fluidized bed while a constant lower temperature was maintained inside the tube by circulating cold water through it. The transducers were stainless steel cylindrical inserts with fast responding and non-intrusive surface thermocouples on their outer face. The thermal properties of the transducer were matched closely to that of heat transfer tube material. The fluxmeter that forms the transducer comprised two 304 stainless steel half-cylinders that had a chromel and an alumel ribbon running along the axis of the composite cylinder. Heat flux was in the axial direction of this composite cylinder. The ribbons were insulated from each other and the half-cylinders by thin sheets of mica. The chromel and alumel ribbons were a part of a K-type thermocouple that was created by joining the ends of the thermocouple wires at a minute spot at the surface. The thermocouple had a low response time to measure accurately any variations in the surface temperature.

McKain *et al.* (1993, 1994) conducted a preliminary investigation which led to the current study by measuring the surface temperatures using a single surface thermocouple. The assembly comprised of a chromel–alumel thermocouple with leads threaded through a small hole in the wall of a 50 mm outside diameter stainless steel heat transfer tube. Differential pressure across the thermocouple was measured by placing two pressure ports, one above the thermocouple and the other below the thermocouple. To test the instrumentation, bubbles were generated below the probe at 3 Hz by solenoid-controlled air bursts and the instantaneous surface temperature and differential pressure across the thermocouple were recorded at a frequency of 120 Hz. Analysis of the differential pressure signal using fast Fourier transforms confirmed that bubbles were generated at a frequency of 3 Hz. Later the heat transfer tube was modified with probes arranged circumferentially around the tube at five different positions and the five surface temperatures were measured simultaneously with sand as the bed particles and air as the fluidizing gas. The differential pressures between two taps were measured using a differential pressure transducer and the signals were also captured at a sampling frequency of 120 Hz.

Karamavruc *et al.* (1994) worked on the comparison of heat transfer coefficients based on the experimental values obtained in the current study by solving numerically the governing heat conduction equations using both one-dimensional (1-D) and two-dimensional (2-D) analyses to interpret the data. The analysis showed that temperature gradients around the tube exist so that different heat transfer coefficients arise for the 1-D and 2-D cases. The local instantaneous heat transfer coefficient for 1-D and 2-D showed considerable difference at lower gas velocities that were closer to minimum fluidizing velocity. At higher gas velocities the frequency of the bubbles in the bed increased and temperature gradient around the circumference of the tube became weaker making the difference in the coefficients as negligible.

Results of previous investigations on the heat transfer coefficients from immersed surface to the bed for particle size equal to or less than 1 mm were reviewed and presented in table 1. It would be expected that average values found in the present study would agree with these average values in the literature.

3. EXPERIMENTAL APPARATUS

The experimental apparatus described below is essentially the same as that used by McKain *et al.* (1993) and McKain (1993) to measure the instantaneous surface temperatures and vertical differential pressures on a hot horizontal tube immersed in a cold fluidized bed.

Fluidized bed

The schematic diagram of the experimental set-up is shown in figure 1. The bed is constructed with 1.3 cm thick clear acrylic and is 30.5 × 30.5 × 61 cm in size. The freeboard of the fluidized bed is capped and is connected to an exhaust system to remove any elutriated particles. The bed has two holes of diameter 51 mm through opposing walls of the vessel to hold the heat transfer tube horizontally in the bed. The center of the immersed horizontal tube was positioned at a height of 14.8 cm from the top of the distributor plate in this study. The bed particles that were used for the study were sieve-sized by a standard sieve shaker and the surface average diameters of the

Table 1. Review of heat transfer coefficients from an immersed surface to the bed for particle size less than 1 mm

Investigators	Tube diameter (mm)	Bed material	Particle diameter (mm)	Gas velocity (m/s)	Heat transfer coefficient ($W/m^2 K$)
Mickley *et al.* (1961)	6.35	spheres	0.04–0.3	0.086	50–525
		glass beads		0.186	50–1350
					$-[h_i(t)]$
Gelperin *et al.* (1969)		sand	0.16, 0.26, 0.35	0.15–1.0	160–330
					$-[\langle h_i \rangle]$
Baskakov *et al.* (1973)	15 & 30	corundum	0.12, 0.32, 0.5	0.04–0.18	530
				0.14–0.6	370
				0.25–0.75	310
					$-[\langle h \rangle]$
Grewal & Saxena (1980)	12.7	sand	0.45	0.21–0.58	260–350
		dolomite	0.29		325–360
		carbide	0.18 and 0.36		340–500 and 250–390
					$-[\langle h_i \rangle]$
Fitzgerald *et al.* (1981)	50.8	dolomite	>0.4	2.75, 2.3	68–210
					74–159
					$-[h_i(t)]$
George (1987)	50.8	beads	0.15	0.33	841
					$-[\langle h \rangle]$
George & Smalley (1991)	50.8	granular	0.9	1.0	324
		refractory			$-[\langle h \rangle]$
					321
					$-[\langle h_i \rangle]$
Khan & Turton (1992)	50.8	sand	0.73	1.2, 1.6 (U_0/U_{mf})	135–773
					144–804
					$-[h_i(t)]$
George (1993)	50.8	granular	1.0	1.0	140–870
		refractory			$-[h_i(t)]$

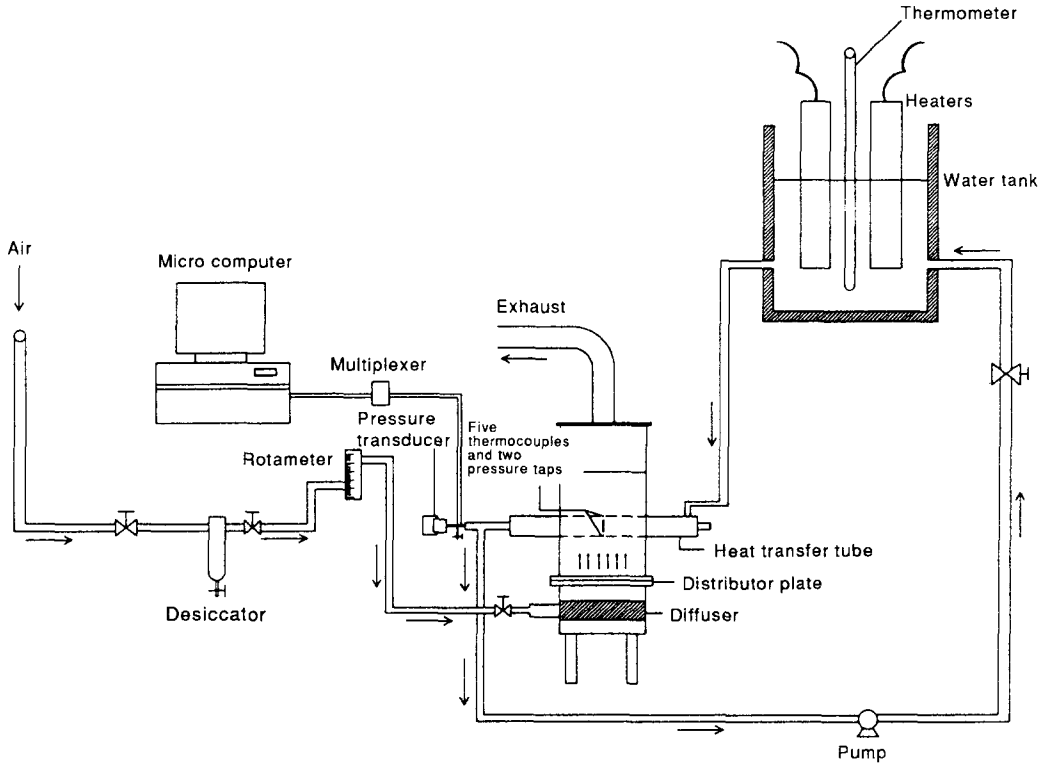

Figure 1. Schematic diagram of the experimental set-up.

particles were calculated and are given in table 2. The bulk bed temperature was maintained well below the tube surface temperature, so that the flux of heat from the tube surface to the bed particles was sufficient to permit accurate measurement of instantaneous surface temperatures. The bed had an air plenum beneath the distributor plate, which had 900 holes of diameter 2.4 mm. The distributor plate was provided with a 200 mesh screen over the plate to prevent any small particles falling through the holes in the plate into the plenum. The plenum was connected to the main air flow line that was controlled by a globe valve located near the entrance of the plenum. The air supply rate was measured using a standard rotameter scaled from 0 to 0.0235 m^3/s for standard temperature and pressure. A desiccator was attached to the air pressure line to prevent excessive moisture from entering the bed. The temperature inside the heat transfer tube was maintained at close to 373 K by drawing hot water into the tube from a surge tank of capacity 0.008 m^3 that was continuously heated by two 1000 W immersion heaters. The hot water was circulated back to the tank using a centrifugal pump. This water flow was throttled using a globe valve connected to the discharge of the pump. The connecting tubes were insulated using Neoprene rubber to reduce heat loss from the tubes. The temperature of the hot water in the tank was measured using a standard mercury thermometer.

Heat transfer tube

The instrumented heat transfer tube used in this research was derived from the tube used by Khan & Turton (1992). It was constructed of 304 stainless steel and comprised of two halves so

Table 2. Physical properties, minimum fluidizing velocity U_{mf} and terminal velocity U_t for the bed particles used

Particle beds	d_{SA} (mm)	U_{mf} (m/s)	$R_{ep,mf}$	Ar	c (kJ/kg K)	Shape and sphericity	U_t (m/s)
Sand1	0.317	0.084	1.77	3004	0.79	0.86, round	2.2
Sand2	0.483	0.184	5.91	10628	0.79	0.86, round	3.2
Abrasive	0.535	0.227	8.10	15000	0.79	0.67, angular	2.6
Glass beads	0.467	0.176	5.48	9422	0.67	1.0, spherical	4.1

that the tube could be split longitudinally for installation of instrumentation. Five surface thermocouples were placed around the circumference of the tube at five different positions at an angle of 45° to one another. The thermocouples were threaded through a 12.7 mm section of stainless steel hypodermic tube till the thermocouple bead protruded about 2.5 cm from the end of the tube section. The thermocouple beads were coated with thermally conductive epoxy adhesive. The coating minimized any adverse thermal effects on the thermocouple probe assembly. The protruding portion of the thermocouple wire that was coated with the epoxy adhesive was carefully drawn into the tube till the tip of the bead was flush with the end of the tube. The thermocouple tube was then inserted into a radial hole drilled through the wall of the heat transfer tube so that the probe was flush with the outer surface of the tube wall. The center thermocouple (located at the side of the tube at an angular position of 0°) was arranged with two pressure sensing taps so that the taps were above and below the thermocouple and separated by a distance of 15.9 mm. The two taps were connected across a Validyne (P305D) differential pressure transducer of range ± 1.20 kPa. In this way one can measure the differential pressure that spans the center thermocouple so that one can infer the presence of a bubble at that point. The theory pertaining to these taps was similar to the dual static pressure probe theory used by Atkinson & Clark (1988) for bubble detection. There was provision to flush the pressure ports periodically using a solenoid controlled purge valve system. Port blockage can cause significant errors in differential pressure measurement. The surface temperatures and differential pressure were taken using a 40 MHz, 80386 microcomputer with Analog Devices, RTI-815 data acquisition board and a 16-channel MUX-16TC multiplexing thermocouple amplifier. Preliminary testing was done by McKain *et al.* (1993) with sand as the bed particles. Variations in the temperature of the tube surface were amplified with a gain of 100, before it passed through a filtering circuit to the RTI board. A gain of 10 on the RTI board with a signal gain of 100 gave an overall gain of 1000, which proved sufficient to make the data from the thermocouples readable. Resistance–capacitance filters on board reduced the high frequency noise picked up by the thermocouple data. A total of 1024 data points were sampled at a sampling frequency of 120 Hz (intervals of 0.00833 s) for a total data acquisition period of 8.53 s. This was considered sufficiently long that measurements of bed characteristics were statistically significant. The transient response time of similarly mounted K-type thermocouples for a step change in the surface temperature was reported by Khan & Turton (1992) to be approximately 10 ms.

Uncertainty for the measured temperatures and heat transfer coefficients were analysed. The noise component in the temperature signal due to external electrical sources was filtered using R-C filters on board. A 120 Hz signal from a transformer circuit was used in all testings to provide a zero crossing sampling trigger to the RTI board to reduce the 60 Hz noise due to electrical signals near to the measuring equipment. The filtering technique reduced the noise to as low to one digital count that corresponded to a noise level of 2.4 mV using a range of ± 5 V on the A/D board, a gain of 1000 and 12 bit resolution (McKain 1992). This noise resulted in a maximum error of ± 0.056°C in the temperature measurement. The error in the air flow is a combination of the manufacturer's accuracy of 4% on the full flow and a reading accuracy of 1 cfm. At worst at the lowest flow rate, this would lead to a 9.8% error on the flow rate. Since the heat transfer is calculated primarily from fluctuating temperatures, the greatest error in temperature that can influence the heat transfer is a digital count, which is 0.056°C. To assess the influence of a misread temperature on the calculated heat transfer coefficient, a value of temperature at one point in the instantaneous trace was lowered by one digital count. The calculated value of $h_i(t)$ at the next time step was changed by 36 W/m^{2}K. This was found to be maximum by conducting the test for different data samples. The temperature of the bed was accurate to 0.7°F and for the smallest value of $(T_{wall} - T_{bed})$, this error can be 2.4%.

Data acquired

As the current study focuses on the heat transfer and the hydrodynamics in the bed, particle beds were classified based on the Reynolds and Archimedes numbers at minimum fluidization. The particle beds were classified as Group I of the powder classification scheme based on Saxena & Ganzha (1984) and Saxena (1989) that corresponds to Geldart (1986) group B particles. Four different Group I particle beds used were sand of two different size distributions (surface average

diameter d_{SA} of 0.317 and 0.483 mm), abrasive and glass beads. The experiments were carried out with four different bed particles at three different bed heights run at various gas velocities. The particles were sieve-sized for calculating the surface average diameter (d_{SA}) using a standard sieve shaker machine having a top screen size of 3.35 mm and bottom screen size of 0.053 mm. The surface average diameter d_{SA} was calculated as,

$$d_{SA} = \frac{1}{\sum_{i=1}^{n} \left(\frac{x}{d_p}\right)_i} \quad [2]$$

where x is the mass fraction of the particles in a size group of diameter d_p. The physical properties of the bed particles are shown in table 2. The bed particles used a fluidized well with vigorous bubbling action at higher ratios of superficial gas velocity to minimum fluidizing velocity. The minimum fluidizing velocity U_{mf} was calculated for these non-spherical particles using the Wen & Yu (1966) correlation

$$\frac{d_p U_{mf} \rho_G}{\mu} = \left[(33.7)^2 + 0.0408 \left(\frac{d_p^3 \rho_G (\rho_p - \rho_G) \boldsymbol{g}}{\mu^2} \right) \right]^{0.5} - 33.7 \quad [3]$$

where μ is the viscosity of the gas, $\boldsymbol{g}$ is the acceleration due to gravity, ρ_p is the density of the particles, ρ_G is the density of the gas and U_{mf} is the minimum fluidizing velocity. The particles were considered to be classified as fine particles because the Reynolds number at minimum fluidizing velocity ($R_{ep,mf}$) was less than 20 as shown in table 2. The minimum fluidizing velocity for the particle beds based on the calculated values agreed with experimental values to $\pm 14\%$. The terminal velocity was calculated using the Haider & Levenspiel (1989) equation developed for the terminal velocity of the particles with sphericity lying between 0.5 and 1.0.

$$u_t^* = \left[\frac{18}{(d_p^*)^2} + \frac{(2.335 - 1.744\phi_s)}{(d_p^*)^{0.5}} \right]^{-1} \quad [4a]$$

$$d_p^* = d_p \left[\frac{\rho_G (\rho_p - \rho_G) \boldsymbol{g}}{\mu^2} \right]^{1/3} \quad [4b]$$

$$u_t = u_t^* \left[\frac{\mu (\rho_p - \rho_G) \boldsymbol{g}}{\rho_G^2} \right]^{1/4}. \quad [5]$$

In [4a] and [4b], d_p^* and u_t^* are dimensionless numbers and although the notion of sphericity Φ_s of any particles is vague, values of 0.86, 0.67 and 1.0 were taken as representative of the shape for sand, abrasive and glass beads , respectively. The terminal velocities of the particles used are given in table 2. The sand particles used were of two different size distributions, having surface average diameters of 0.317 mm (denoted as "sand1") and 0.483 mm (denoted as "sand2"). The sand1 particles were run at superficial gas velocities of 0.155, 0.179 and 0.202 m/s, sand2 at 0.213, 0.24 and 0.267 m/s, abrasive at 0.293, 0.323 and 0.352 m/s and glass beads at 0.264, 0.294 and 0.323 m/s at three different bed heights of 20, 23 and 26 cm measured from the distributor level to the surface of the bed particles at minimum fluidizing condition.

4. THEORY—DEDUCTION OF HEAT TRANSFER COEFFICIENT

The instantaneous radial heat flux and local heat transfer coefficient at any axial and circumferential point on an immersed tube are calculated by solving the unsteady heat conduction equation within the tube wall material. The outer boundary condition is a surface temperature that fluctuates with time. The inner surface of the tube is maintained at constant temperature, in our case 373 K. The governing heat condition equation can be written as,

$$\frac{1}{r} \frac{\partial}{\partial r} \left[kr \left(\frac{\partial T}{\partial r} \right) \right] = c\rho \left(\frac{\partial T}{\partial t} \right) \quad [6]$$

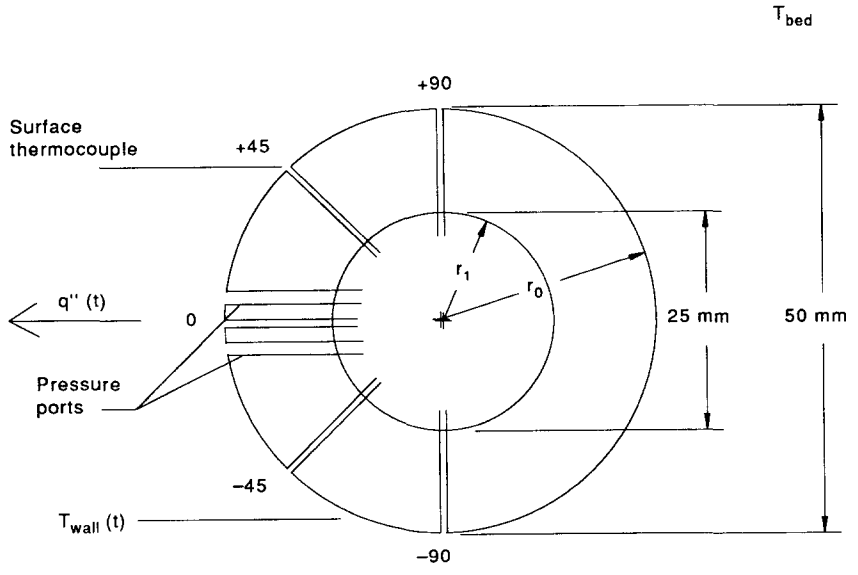

Figure 2. Cross-section of the heat transfer surface.

where k is the thermal conductivity of the tube material, c is the heat capacity of the tube material and ρ is the density of the tube material. The cross-section of the heat transfer tube used in this study is shown in figure 2. The governing boundary conditions are

inside wall temperature $= T(r_i, t) = T_{fluid} =$ constant
outside wall temperature $= T(r_o, t) = T_{wall}(t)$
radial temperature profile $= T(r, 0) = T(r)$

r_i and r_o are the inner and outer radii of the tube, T_{fluid} is the constant temperature of the fluid circulated inside the heat transfer tube and $T_{wall}(t)$ is the surface temperature that fluctuates with time. The surface is continuously exposed to the air flow and emulsion phase. Excess gas moves through the emulsion in the form of bubbles that bring the heated surface into contact with fresh particles periodically and make the surface temperature fluctuate with time. The initial condition across the tube wall was taken as a steady state temperature distribution across the tube surface with inner constant wall temperature and average outer temperature obtained from the measured data. At the beginning, the initial condition distorts the time-varying temperature profile across the tube surface. For the present application, after a period of 6 s the initial effect is damped out and the solution is independent of the initial conditions (Karamavruc *et al.* 1994). However, a period of 1.75 s of the initial temperature profile was excluded while performing the instantaneous heat transfer coefficient calculations.

The differential equation [6] is solved numerically using the fully-implicit method, where the domain is divided into non-overlapping control volumes which are independently surrounded by grid points as solved by Karamavruc *et al.* (1994). The resulting solution obtained by this method implies that the total conservation of energy is satisfied by any control volume and over the whole calculation domain. The discretized equation is achieved by integrating [6] over the control volume and a time interval from t to $t + \Delta t$. The local heat transfer coefficient is calculated by equating the local instantaneous heat flux from the tube surface to the heat flux into the fluidized bed,

$$-k\left(\frac{\partial T}{\partial r}\right)_{\text{at } r = r_o} = h_i(t)[T_{wall}(t) - T_{bed}]. \qquad [7]$$

The time-averaged local heat transfer coefficient $\langle h \rangle$ is calculated by averaging the local instantaneous heat transfer coefficient over a period of time corresponding to n number of time intervals

$$\langle h \rangle = \frac{\sum_{i=1}^{n} h_i(t)}{n}. \qquad [8]$$

5. EXPERIMENTAL RESULTS

Local instantaneous surface temperatures

Local instantaneous surface temperatures at five different locations and the differential pressure across the center thermocouple are obtained for all four bed particles (sand1, sand2, abrasive and glass beads) at different bed heights and flow velocities. Figure 3 shows the plot of instantaneous surface temperature and differential pressure for sand1 bed particles at a bed height of 20 cm above the distributor plate at a superficial gas velocity U_0 of 0.155 m/s, that is, $U_0/U_{mf} = 1.84$. As shown in figure 3, the variation of the surface temperature with respect to time is minimal for the top two

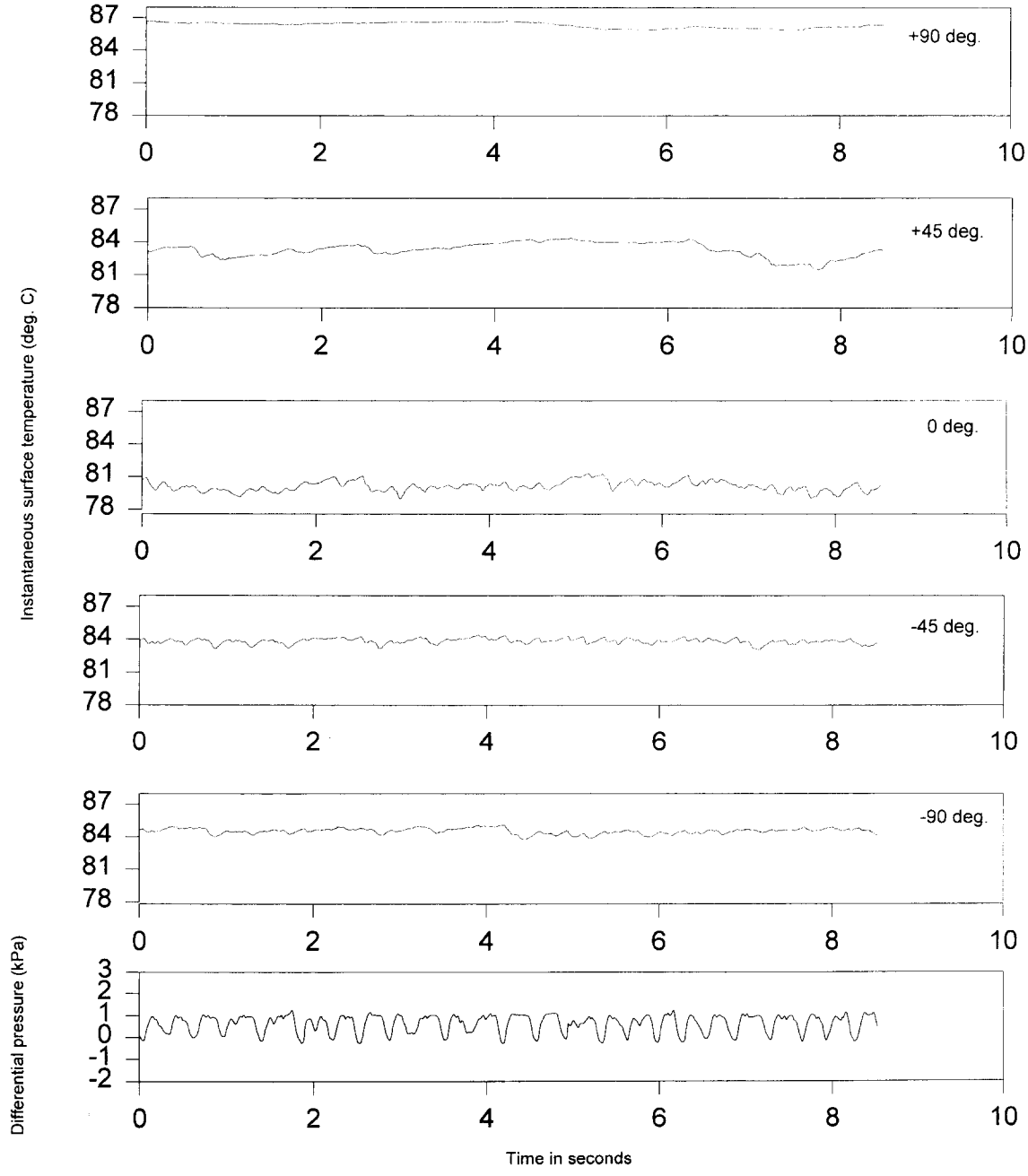

Figure 3. Time-varying local surface temperatures and differential pressure data for sand1 particles at a bed height of 20 cm and gas velocity of 0.155 m/s.

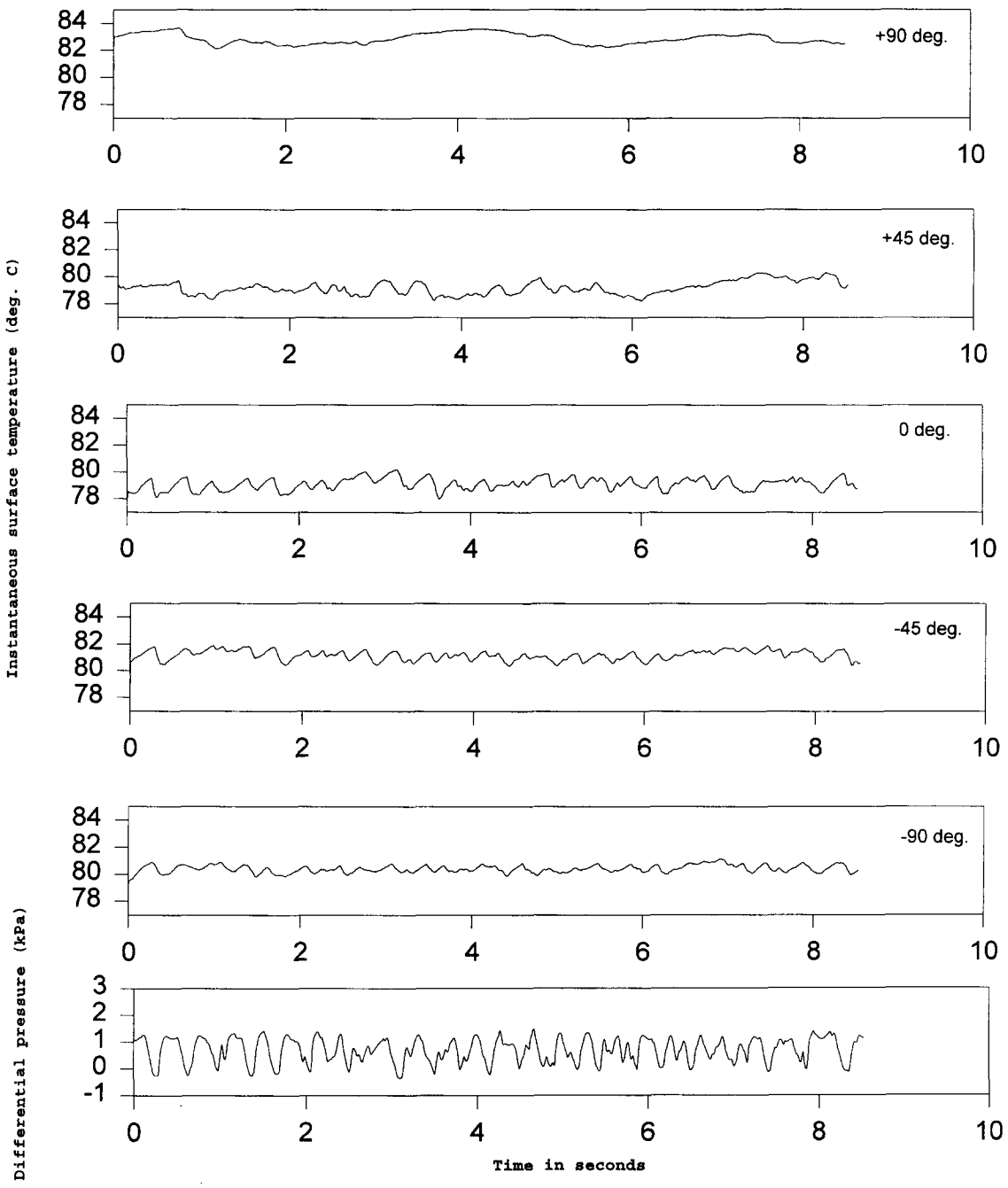

Figure 4. Time-varying local surface temperatures and differential pressure data for sand1 particles at a bed height of 20 cm and gas velocity of 0.202 m/s.

thermocouples (+90 and +45°). This is due to low gas superficial velocity, where stagnant bed particles reside on the top of the tube. Fundamental theory (Mickley & Fairbanks 1955) argues that a major heat transfer mechanism is by particle packet movement so that stagnant particles lead to few fluctuations of the heat transfer coefficient since they represent a conduction mode of transfer. It is also seen from figure 3 that an instability occurred in the surface temperature for the top two thermocouples after a period of about 6.25 s. This is ascribed to removal of the hot stagnant particles by the movement of a passing void and their replacement by a packet of cold particles that has a higher rate of heat transfer at that particular period of time. The stagnation

phenomenon is not seen in the case of the bottom thermocouples. Stagnation of the particles on the upper tube surface was also observed by Catipovic (1979) and Khan & Turton (1992) at low ratios of superficial gas velocity to minimum fluidization velocity. Figure 4 shows the surface temperatures and the differential pressure plot for sand1 particles at a bed height of 20 cm and a superficial gas velocity of 0.202 m/s ($U_0/U_{mf} = 2.41$) at which the bed bubbles move vigorously. In figure 4 the top two thermocouples show higher thermal activity which is due to the movement of the bubbles that replace the stagnant particles with fresh particles more frequently than at lower gas flow rates.

Bubble frequency

The instantaneous surface temperatures are auto-correlated for every thermocouple to calculate the frequency of the major heat transfer events in the bed. The auto-correlation is used to infer the frequency of the bubbles. One may determine a correlation coefficient C_{at}, for a phase shift Δt given by

$$C_{\Delta t} = \frac{\sum_{\Delta t = 0}^{t_{max} - \Delta t} [T(t) \cdot T(t + \Delta t)]}{\sum_{\Delta t = 0}^{t_{max} - \Delta t} [T(t) \cdot T(t)]} \qquad [9]$$

where $T(t)$ is the time-varying surface temperature of the thermocouples. The correlation coefficient is unity when the phase shift is zero and the correlation coefficient decreases for the increase in the phase shift until the original and shifted data are anti-correlated. Further increase in the phase shift for periodic signals increases the correlation coefficient where it reaches a maximum when the original and shifted data are correlated. The inverse value of the phase shift at this point gives the dominant frequency of thermal events (interpreted as bubble events) in that set of data. In a freely bubbling bed, there may be some concern in using the auto-correlation function to infer the bubble frequency, since the notion of bubble location relative to the measurement is uncertain (Werther

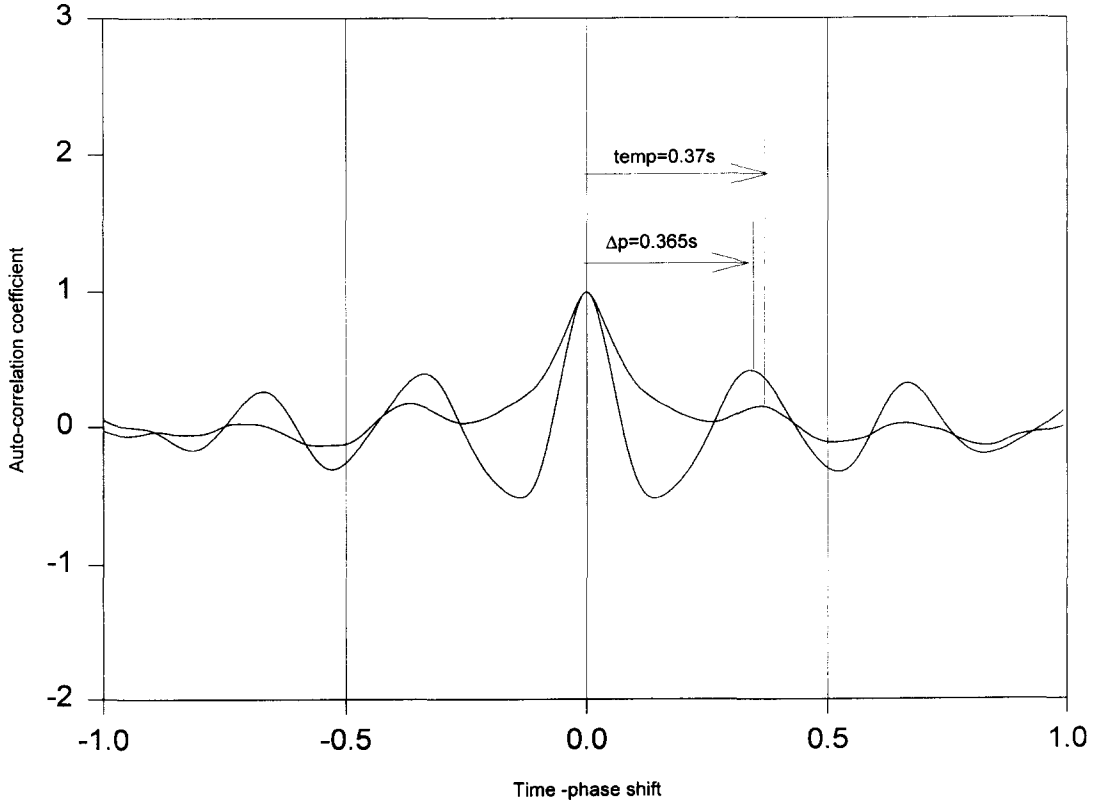

Figure 5. Auto-correlation of the surface temperature and differential pressure data for sand1 particles at a bed height of 20 cm and gas velocity of 0.155 m/s.

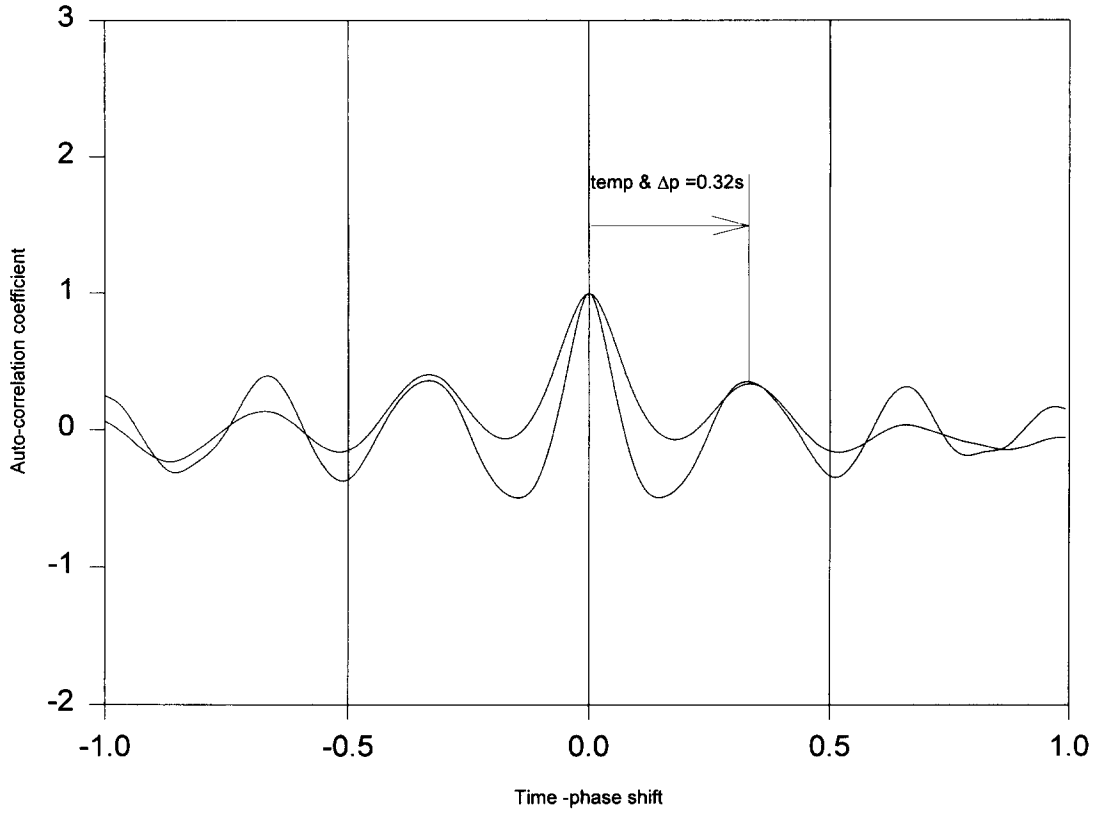

Figure 6. Auto-correlation of the surface temperature and differential pressure data for sand1 particles at a bed height of 20 cm and gas velocity of 0.202 m/s.

& Molerus 1973). Although the bubble frequency is not well defined, the authors believe that it is a somewhat more precise concept at a surface and have chosen the auto-correlation function as a representative measure of the bubble frequency. The cross-correlation of temperature and differential pressure is also done in a similar way by correlating the temperature and the differential pressure measurements. Since heat transfer and bubble events are argued to be intimately related, these two frequencies should match well, as was found in most cases in a previous study (McKain *et al.* 1993). Figures 5 and 6 show the auto-correlation for the center thermocouple and differential pressure for sand1 particles at a bed height 20 cm at a superficial gas velocity of 0.155 m/s (see figure 3) and 0.202 m/s (see figure 4), respectively. The frequencies of the center thermocouple and differential pressure measurements are compared in figure 7 and are found to match closely.

Figure 8 shows the increase in the bubble frequency for the center thermocouple for increase in the gas velocity for the various bed particles at a bed height of 20 cm. It is seen that the bubble frequency based on temperature data for the side thermocouple (located at 0°) increased with increase in gas superficial velocity. This is due to increase in bubble generation and hence movement of the particles at higher superficial velocities. Also at higher gas velocities, a larger volume of gas flows through the bed and causes the volume of the bubbles to increase so that they in turn rise with a higher velocity. This phenomenon is observed in all four bed particle types. Cross-correlation for two sets of temperature data lead to the determination of bubble rise velocity. Figure 9 shows the cross-correlation of the thermocouple located at 0° with +45° and −45° with 0°. As there was a time delay between the thermocouple signals, the correlation curve shifted from the center. This time phase shift gave time for the bubble to cross the circumferential distance between the thermocouples that were cross-correlated. Based on the distance between thermocouples and time phase shift, the calculation yielded a bubble rise velocity (U_{br}) of 59.5 cm/s. This corresponded to a bubble diameter (d_b) of 7.14 cm using the relation between rise velocity and bubble diameter (Kunii & Levenspiel 1992). Bubbles of this approximate size were visually observed in the bed.

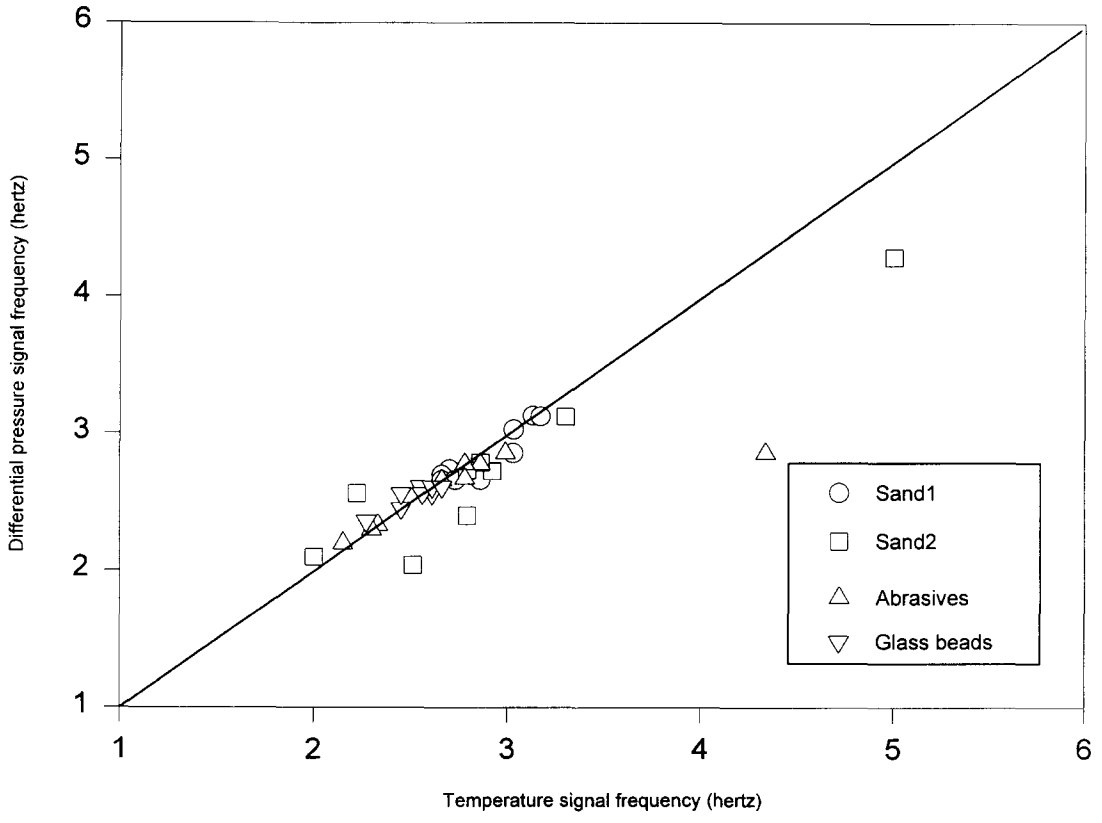

Figure 7. Comparison of bubble frequencies based on auto-correlation of instantaneous surface temperature and differential pressure data.

Local instantaneous heat transfer coefficient

The local instantaneous heat transfer coefficients are calculated from the instantaneous surface temperatures for all five angular positions using the 1-D numerical analysis presented above. Karamavruc *et al.* (1994) have shown that the 1-D and 2-D cases agree typically within 16% for the side thermocouple (at 0°) and 29% for other thermocouples. In figures 3 and 4, the instantaneous surface temperatures are seen to be a minimum at the side of the tube (0°) which infers a higher heat transfer rate at this zone. Figures 10 and 11 show the plot for the local instantaneous heat transfer coefficient for all angular positions for sand1 bed particles. At lower gas velocities the magnitude of fluctuations for the top thermocouple is smaller due to the stagnant zone on top of the tube. Better contact with the emulsion phase and the tube surface is established at higher gas velocities due to improved solids motion on the top of the tube. At increased gas velocity the magnitude of fluctuations increases dramatically for the top portion of the tube (+90°) which is due to the breaking of the stagnant zone by the frequent passing voids. The results are compared with previous published work, although the conditions are not identical to those used in the present study. Glass beads showed a minimum of 273.2 to a maximum of 513.2 W/m^2 K at a gas velocity of 0.323 m/s. This differs from the value of Mickley *et al.* (1961) for a size range of 0.043–0.32 mm that ranged from a minimum of 50 to a maximum of 525 W/m^2 K. Sand2 bed particles showed a minimum of 316 to a maximum of 526 W/m^2 K at a gas velocity of 0.267 m/s for the side of the tube surface. This was higher compared to Fitzgerald *et al.* (1981) where the values ranged from a minimum of 50 to a maximum of 210 W/m^2 K for a gas velocity of 0.275 m/s. This could be due to the larger particle size used by the previous investigator. The minimum and maximum values when compared to George (1993) were lower and this could have been due to higher gas velocities and radiative heat transfer, whereas the current study is with lower gas velocities and is for a cold bed. However, one must note that the value of the heat transfer

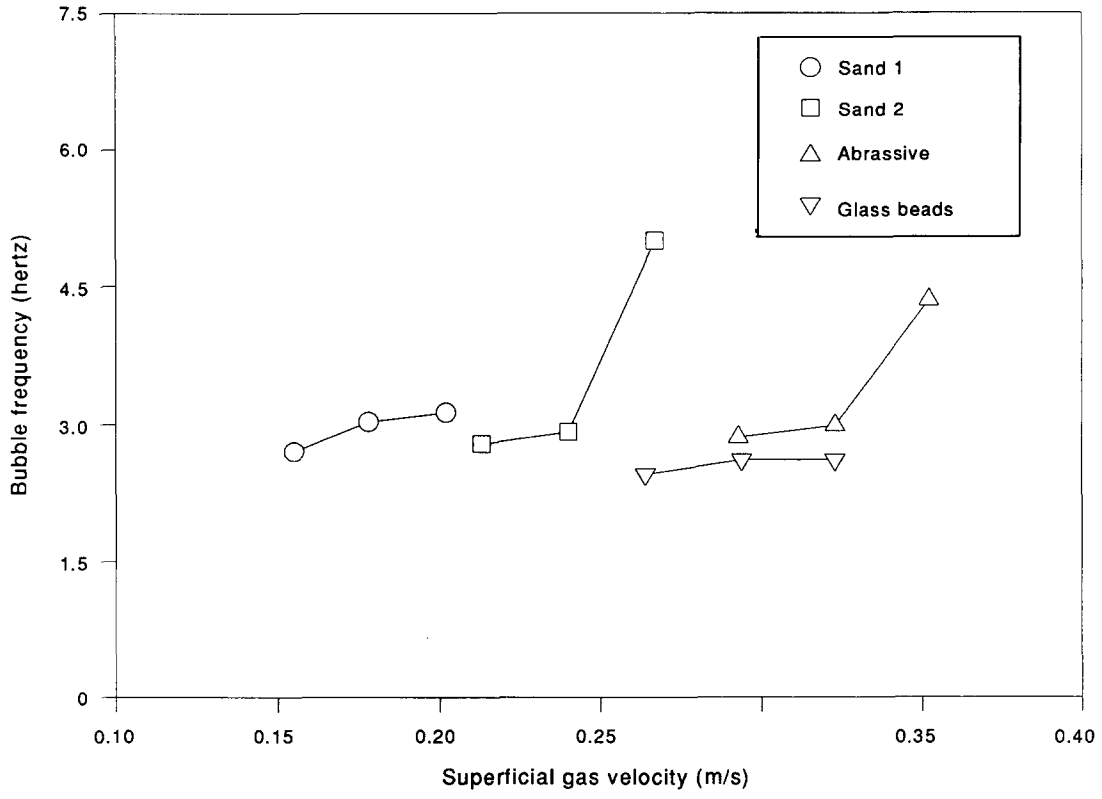

Figure 8. Bubble frequency for center thermocouple versus gas velocity for four types of bed particles at a bed height of 20 cm.

coefficient is governed not only by superficial gas velocity and particle size, but by a host of other hydrodynamic and geometric factors.

Local time-average and tube-average heat transfer coefficients

Local time-averaged heat transfer coefficients for all angular positions are shown in tables 3 and 4. Figure 12 shows the time-averaged heat transfer coefficients for the sand1 bed particles at five angular positions at three different flow rates for a bed height of 20 cm. The time-averaged heat transfer coefficient values are seen to be maximum at the center (0°) thermocouple. The time-averaged heat transfer coefficient increases for increasing gas velocity due to increased replacement of particles on the tube. Increase in gas velocity had a greater effect on the time-average heat transfer coefficients for the top and bottom portions of the tube. This was also observed by Catipovic (1979) in cold beds and Khan & Turton (1992) in high temperature beds. The tube-average heat transfer coefficient for the whole tube $\langle h_t \rangle$ is calculated as,

$$\langle h_t \rangle = \frac{h_{+90} + 2h_{+45} + 2h_0 + 2h_{-45} + h_{-90}}{8} \quad [10]$$

and the values for each of the four bed particle types are given in table 5. The maximum tube-average heat transfer coefficient for all four bed particles was compared with other investigators in figure 13. The maximum tube-average Nusselt and Archimedes numbers are computed by using the following equations:

$$\overline{\mathrm{Nu}_{\max}} = \frac{d_p \langle h_t \rangle_{\max}}{k_G} \quad [11]$$

$$\mathrm{Ar} = \frac{g d_p^3 (\rho_p - \rho_G)\rho_G}{\mu^2}. \quad [12]$$

The correlations valid for the Archimedes number range developed by Zabrodsky *et al.* (1974) and Varygin *et al.* (1966) were used for the comparison. The data reported in the current study were well within the range predicted by the correlations.

Root mean square (amplitude) of heat transfer fluctuations

Instantaneous heat transfer coefficients $h_i(t)$ are decomposed into an averaged heat transfer coefficient (interpreted as time-average) and a fluctuating component $h_i'(t)$, such that

$$h_i(t) = \langle h \rangle + h_i'(t). \quad [13]$$

The mean value of the fluctuating quantity can be defined as,

$$\overline{h_i'} = \operatorname{Lim}_{\tau \to \infty} \int_{t_0}^{t_0 + \tau} [h_i(t) - \langle h \rangle] \, dt = 0. \quad [14]$$

The root mean square value (amplitude) of fluctuations is calculated by finding the square root of the variance (σ^2) of the fluctuations,

$$h_{rms} = (\sigma^2)^{0.5}. \quad [15]$$

Figure 14 shows the amplitude of the heat transfer fluctuations for the center thermocouple located at 0° for all the four bed particles at different bed heights and gas velocities. It can be observed generally that the amplitude increased for increasing gas velocity for a particular bed height for sand1, sand2 and beads. The amplitude decreased for abrasive for increasing gas velocities at two bed heights even though their time-averaged heat transfer coefficients increased for higher gas

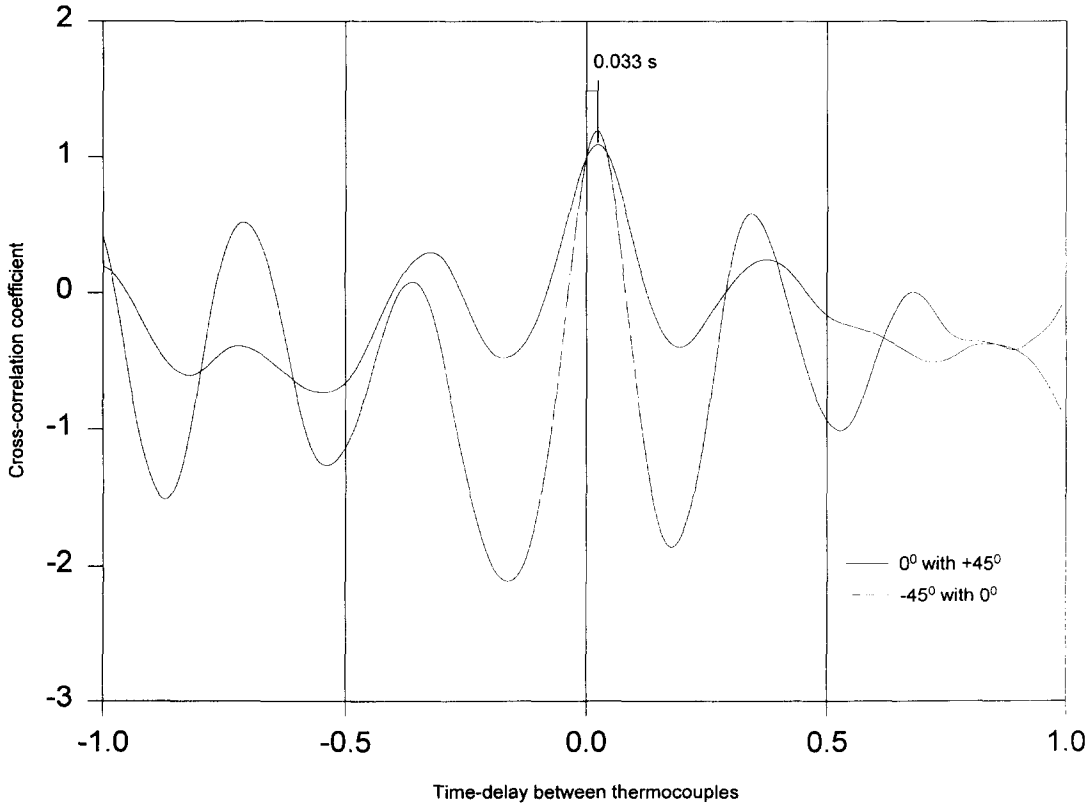

Figure 9. Cross-correlation of adjacent thermocouples (0° with +45° and −45° with 0°) for sand1 particles at a bed height of 20 cm and gas velocity of 0.202 m/s.

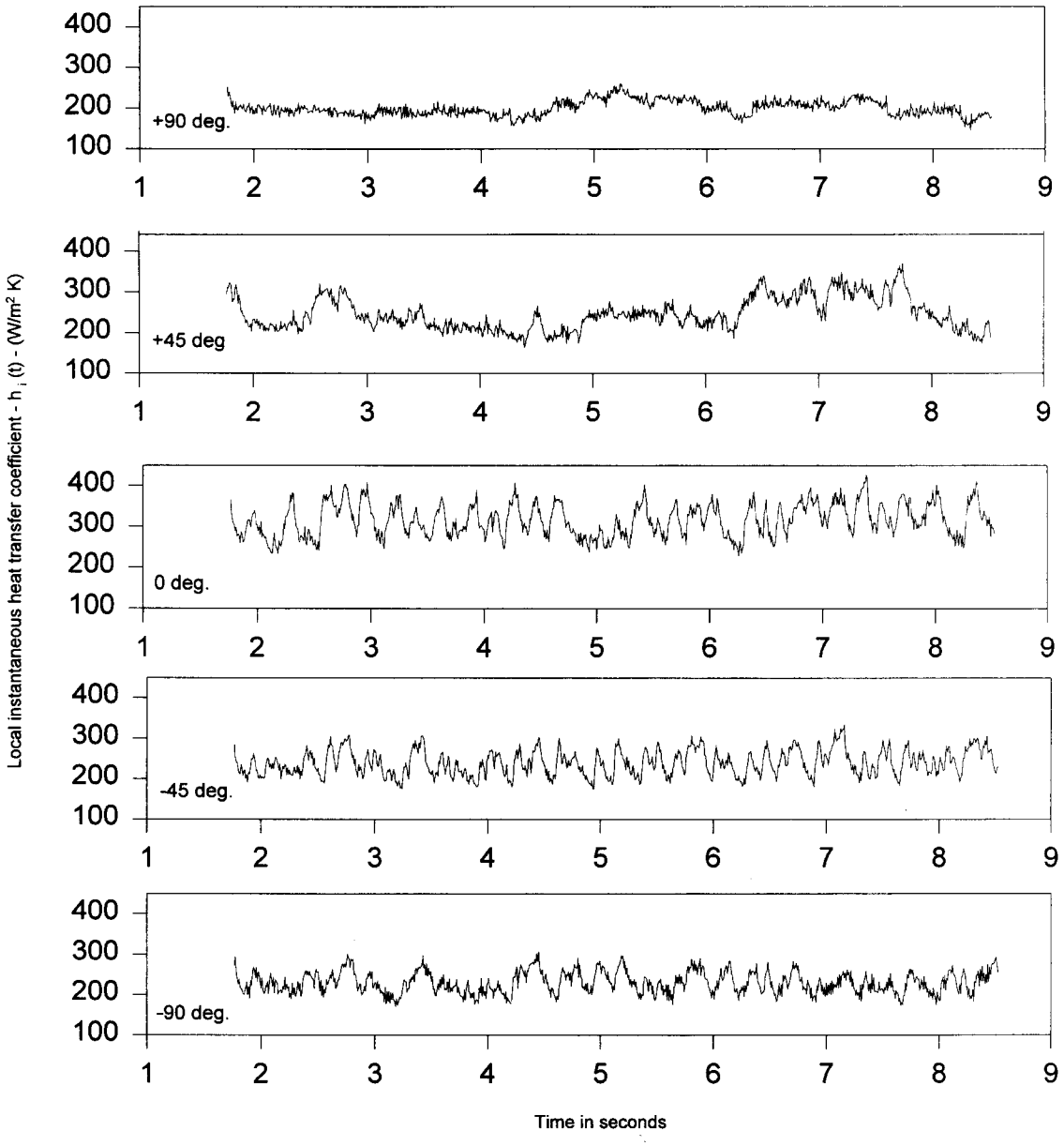

Figure 10. Local instantaneous heat transfer coefficient for sand1 particles at a bed height of 20 cm and gas velocity of 0.155 m/s for all five angular positions.

velocities. This may be explained by the fact that the ratio of heat taken up by the fluidizing gas to the heat taken up by the particles increases as the particle size increases: the abrasives were the largest particles. Figure 15 shows the time-averaged heat transfer coefficients for the thermocouple located at 0° for all the bed particles at different bed heights and gas velocities to compare with the amplitude of heat transfer fluctuations. Generally one can argue that $\langle h \rangle$ and the root mean square average of h_i' vary in sympathy, which is in support of a packet renewal theory of heat transfer.

6. DISCUSSION AND CONCLUSION

The heat transfer in the bed showed results that varied at different angular positions around the tube because the contact characteristics of the emulsion phase with the tube wall are not the same

at all angular positions. By auto-correlating and cross-correlating the time-varying surface temperature and differential pressure data, the bubble frequencies were calculated at different gas superficial velocities. Cross-correlation of adjacent thermal events allowed the researchers to calculate bubble rise velocity and bubble diameter in the bed. It is seen that the bubble frequency increases with the increase in the gas superficial velocity due to greater availability of excess gas free to rise through the bed as bubbles. The heat transfer rate is higher at increased gas velocity as the bubbles replace the particles on the surface with fresh cold "packets" of particles more frequently. The dominant frequencies that are determined to represent the temperature and the pressure data match with each other, thus confirming the relationship between bubble passage and

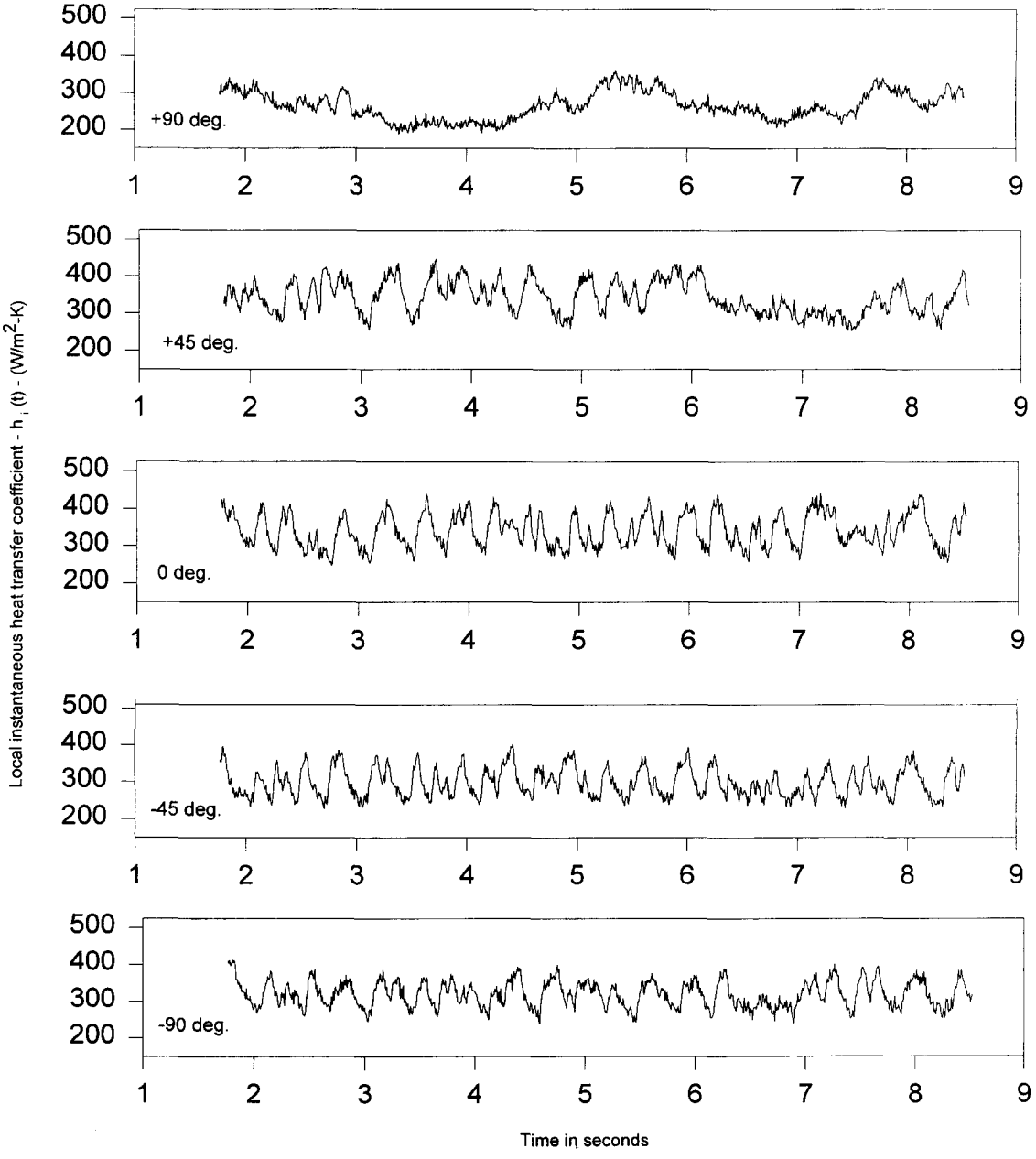

Figure 11. Local instantaneous heat transfer coefficient for sand1 particles at a bed height of 20 cm and gas velocity of 0.202 m/s for all five angular positions.

Table 3. Local time-averaged heat transfer coefficients for sand1 and sand2 particles at five different angular positions at three different bed heights for three different superficial gas velocities

Bed height and angles (deg.)		Time-averaged heat transfer coefficients (W/m^2-K)					
		Sand1 (U_0 in m/s)			Sand2 (U_0 in m/s)		
		0.155	0.179	0.202	0.213	0.240	0.267
20 cm	+90	199.33	224.03	263.94	123.41	324.10	310.33
	+45	244.42	264.22	345.93	233.28	362.85	451.77
	0	315.31	322.21	342.05	292.24	370.45	424.54
	−45	238.63	253.36	298.58	190.12	307.77	335.98
	−90	228.98	267.80	320.56	163.10	318.63	266.46
23 cm	+90	116.16	125.61	149.02	128.63	178.23	290.14
	+45	163.34	147.87	171.71	334.32	346.77	401.75
	0	331.26	322.74	341.29	374.85	382.66	359.17
	−45	234.53	260.89	270.25	275.62	273.43	270.18
	−90	218.67	276.92	316.06	231.59	228.08	267.42
26 cm	+90	150.87	181.74	219.19	174.49	120.19	293.21
	+45	210.84	272.01	341.23	278.05	346.85	416.94
	0	351.17	382.54	390.59	311.90	375.08	366.86
	−45	274.96	296.03	299.00	250.91	276.89	263.64
	−90	299.62	312.13	335.72	253.90	221.23	253.70

Table 4. Local time-averaged heat transfer coefficients for abrasive and glass bead particles at five different angular positions at three different bed heights for three different superficial gas velocities

Bed height and angles (deg.)		Time-averaged heat transfer coefficients (W/m^2-K)					
		Abrasive (U_0 in m/s)			Glass beads (U_0 in m/s)		
		0.293	0.323	0.352	0.264	0.294	0.323
20 cm	+90	279.32	280.08	275.95	223.65	300.33	298.21
	+45	249.17	249.97	284.11	361.34	401.10	413.98
	0	296.52	280.03	310.52	352.21	385.51	385.67
	−45	283.86	298.26	286.08	236.55	282.55	324.50
	−90	254.21	260.99	256.64	197.33	240.08	275.16
23 cm	+90	254.16	265.55	278.69	263.77	275.25	302.52
	+45	297.39	305.87	280.79	351.474	413.46	428.27
	0	283.35	288.23	295.73	359.52	378.71	399.68
	−45	235.24	258.57	275.61	248.14	258.00	286.68
	−90	211.98	226.77	242.76	207.70	217.83	236.92
26 cm	+90	255.65	272.69	284.61	344.22	366.45	416.16
	+45	299.29	301.65	272.05	444.75	452.73	501.50
	0	275.69	282.18	297.99	452.52	451.41	478.20
	−45	235.75	258.77	270.09	310.83	298.75	327.54
	−90	231.69	243.74	252.06	253.47	248.54	271.71

Table 5. Averaged heat transfer coefficients for the whole tube for four types of bed particles

Bed particle	U_0 (m/s)	Tube average heat transfer coefficients (W/m^2-K)		
		Bed height (cm)		
		20	23	26
Sand1	0.155	253.12	224.14	265.55
	0.179	271.42	233.19	299.38
	0.202	319.70	253.95	327.07
Sand2	0.213	214.72	291.22	263.76
	0.240	340.61	301.50	292.38
	0.267	375.17	327.47	330.22
Abrasive	0.293	274.08	262.26	263.60
	0.323	272.69	274.71	275.20
	0.352	286.75	278.21	277.12
Glass beads	0.264	290.14	298.72	376.74
	0.294	334.84	324.18	377.60
	0.323	352.71	346.10	412.80

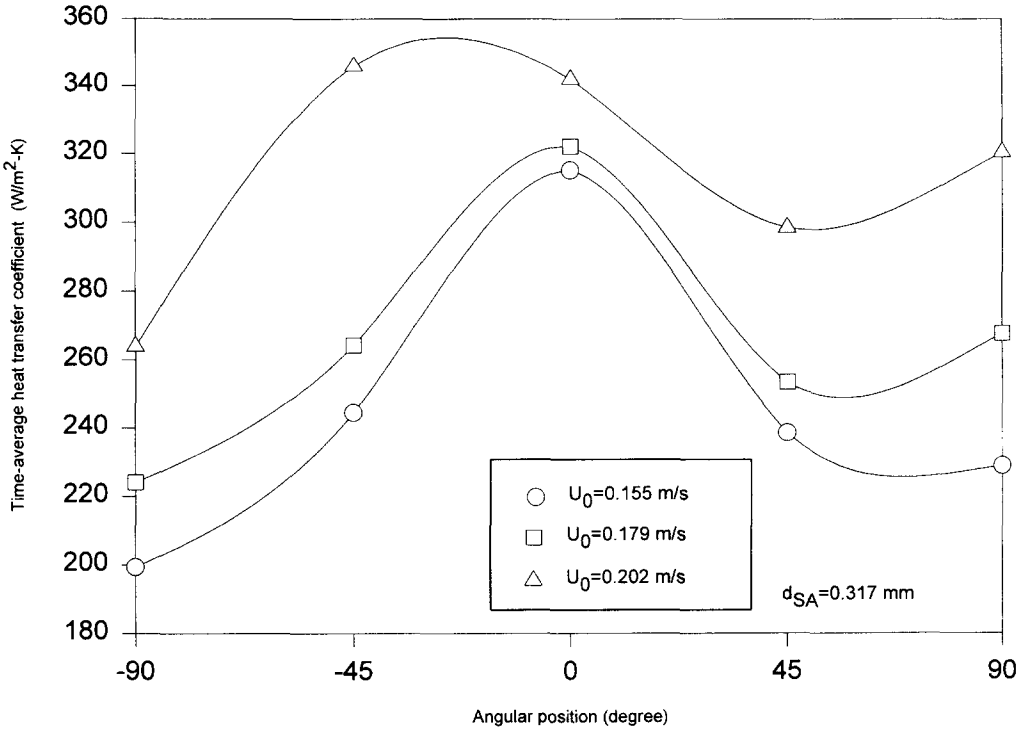

Figure 12. Local time-averaged heat transfer coefficient versus the angular positions for sand1 particles at a bed height of 20 cm at three different gas velocities.

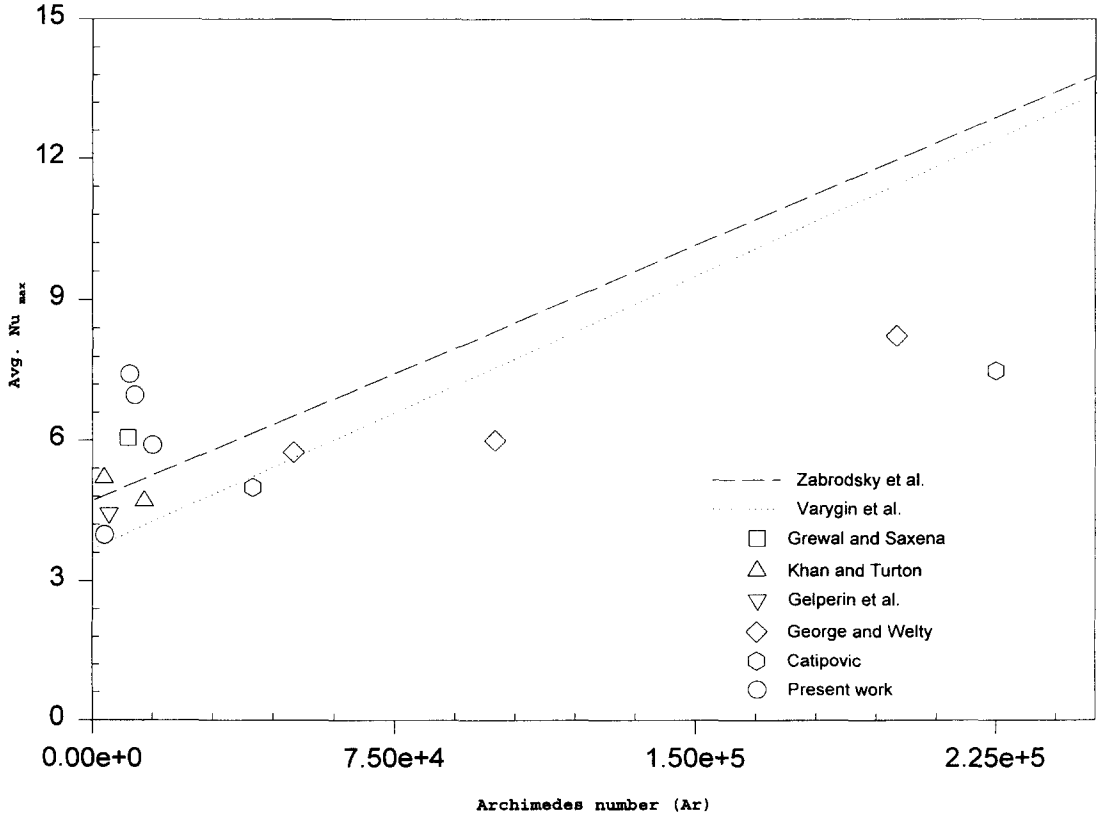

Figure 13. Comparison of maximum tube-average Nusselt number vs Archimedes number—current study and other works are compared to the correlations of Zabrodsky *et al.* (1974) and Varygin *et al.* (1966).

"packet" renewal. The local time-averaged heat transfer coefficients are maximum at 0° for sand1 particles, and at 0° and +45° for other particles. Increased gas velocities showed increase in time-averaged heat transfer coefficients for the tube. Smaller particle sizes were associated with higher magnitudes of fluctuations in instantaneous heat transfer coefficients. Maximum tube-average heat transfer coefficients agree with those available in the literature. The amplitude of heat transfer fluctuations increased for increase in the gas velocity for sand1, sand2 and beads and decreased in two cases for abrasive particles. This method of measuring the heat transfer coefficient for the surface immersed in the fluidized bed is seen to be successful and the averaged data obtained are in good agreement with the available literature. The transient data reported are well suited to a future phenomenological study of fluid bed heat transfer which may lead to a more sophisticated packet renewal model than those currently available.

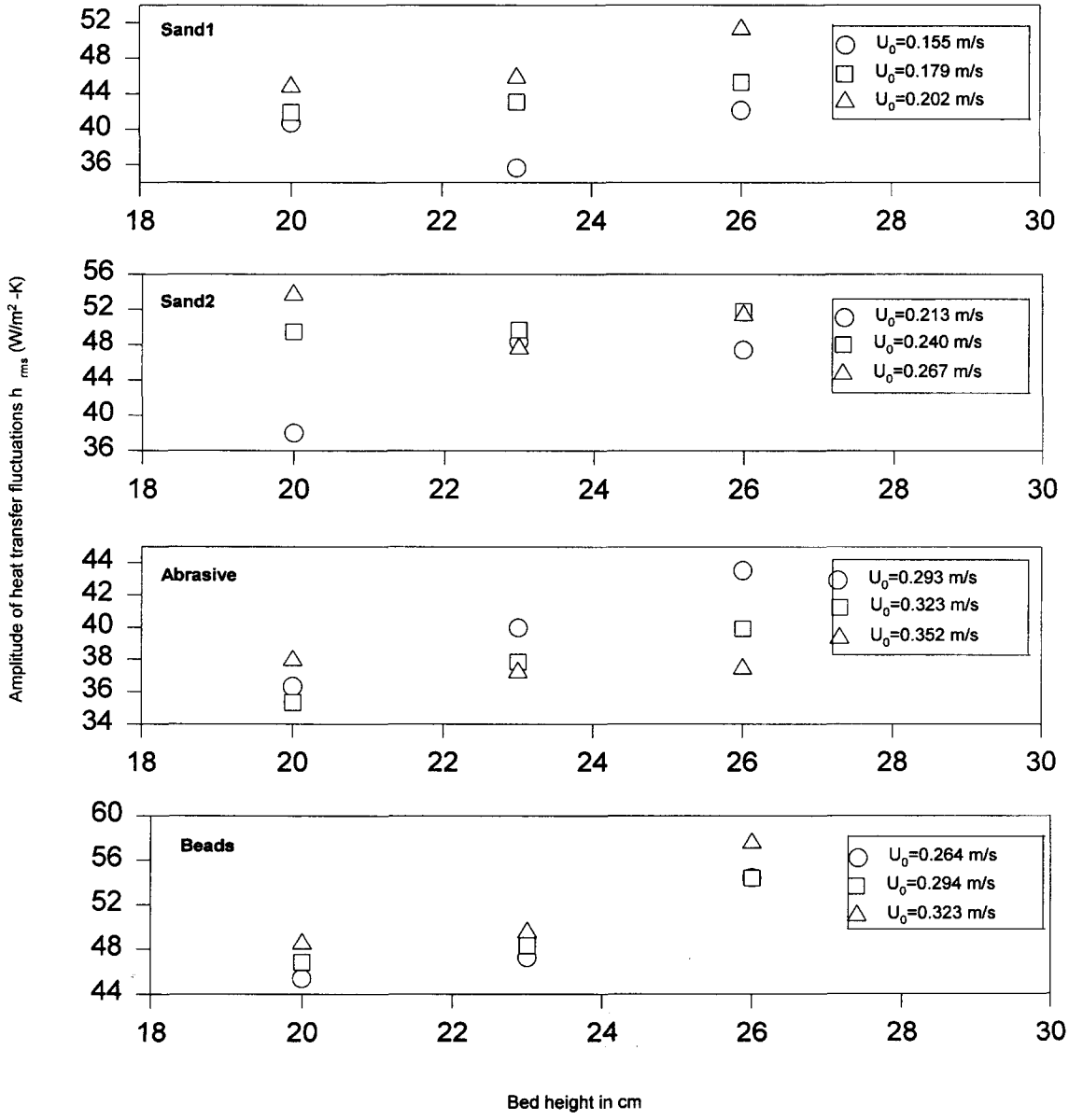

Figure 14. Root mean square (amplitude) of heat transfer fluctuations for center thermocouple versus bed heights for different superficial gas velocities for four bed particles.

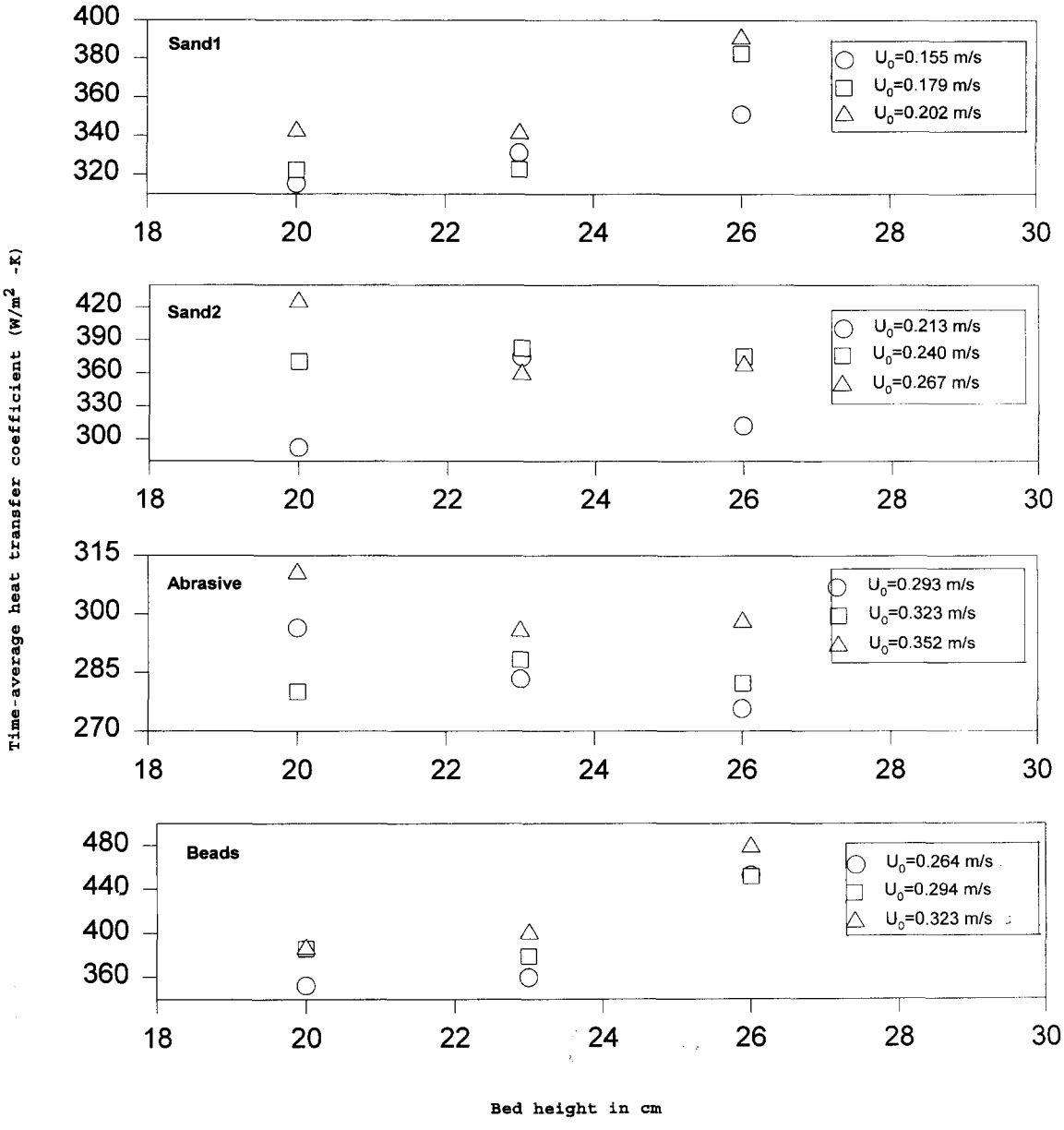

Figure 15. Time-averaged heat transfer coefficient for center thermocouple versus bed heights for different superficial gas velocities for four bed particles.

Acknowledgements—This work has been supported by the National Science Foundation under grant CTS 8957146. The authors wish to thank David McKain for original instrumentation of the tube, Ali Ihsan Karamavruc for assisting in the heat transfer analysis and Dr Richard Turton for his help and insight.

REFERENCES

Atkinson, C. M. & Clark, N. N. 1988 Gas sampling from fluidized beds: a novel probe system. *Powder Technol.* **54,** 59–70.

Baskakov, A. P., Berg, B. V., Vitt, O. K., Filippovsky, N. F., Kirakosyan, V. A., Goldobin, J. M. & Maskaev, V. K. 1973 Heat transfer to objects immersed in fluidized beds. *Powder Technol.* **8,** 273–282.

Botterill, J. S. M. 1975 *Fluid-bed Heat Transfer*, pp. 245–263. Academic Press, London.

Catipovic, N. M. 1979 Heat transfer to horizontal tubes in fluidized beds: experiment and theory. Ph.D. thesis, Oregon State University, Coravallis, OR.

Davidson, J. F. 1963 *Fluidized Particles*. Cambridge University Press, Cambridge, England.

Fitzgerald, T. J., Catipovic, N. M. & Jovanovic, G. N. 1981 Instrumented cylinder for studying heat transfer to immersed tubes in fluidized beds. *Ind. Engng Chem. Fundam.* **20,** 82–88.

Geldart, D. 1986 *Gas Fluidization Technology*. Wiley, New York.

Gelperin, N. I., Ainstein, V. G. & Korotyanskaya, L. A. 1969 Heat transfer between a fluidized bed and staggered bundles of horizontal tubes. *Int. Chem. Engng* **9,** 137–142.

George, A. H. & Welty, J. R. 1984 Local heat transfer coefficients for a horizontal tube in a large particle fluidized bed at elevated temperature. *AIChE Jl* **30,** 482–485.

George, A. H. 1987 A transducer for the measurement of instantaneous local heat flux to surfaces immersed in high temperature fluidized beds. *Int. J. Heat Mass Transfer* **30,** 763–769.

George, A. H. & Smalley, J. L. 1991 An instrumented cylinder for the measurement of instantaneous local heat flux in high temperature beds. *Int. J. Heat Mass Transfer* **34,** 3025–3036.

George, A. H. 1993 Instantaneous local heat transfer coefficients and related fequency spectra for a horizontal cylinder in a high temperature fluidized bed. *Int. J. Heat Mass Transfer* **36,** 337–345.

Grewal, N. S. & Saxena, S. C. 1980 Heat transfer between a horizontal tube and a gas–solid fluidized bed. *Int. J. Heat Transfer* **23,** 1505–1519.

Grewal, N. S. & Saxena, S. C. 1980 Maximum heat transfer coefficient between a horizontal tube and a gas–solid fluidized bed. *Ind. Engng Chem. Process Des. Dev.* **20,** 109–116.

Haider, A. & Levenspiel, O. 1989 Drag coefficient and terminal velocity of spherical and nonspherical particles. *Powder Technol.* **58,** 63–70.

Karamavruc, A., Clark, N. N. & McKain, D. L. 1984 Deduction of fluid bed heat transfer coefficients using one and two dimensional analyses. *Powder Technol.* **80,** 83–91.

Khan, T. 1989 A probe for heat transfer coefficient measurement, M.Sc. thesis, West Virginia University, Morgantown, WV.

Khan, T. & Turton, R. 1992 The measurement of instantaneous heat transfer coefficients around the circumference of a tube immersed in a high temperature fluidized bed. *Int. J. Heat Mass Transfer* **35,** 3397–3406.

Kunii, D. & Levenspiel, O. 1992 *Fluidization Engineering*, pp. 313–326. Butterworth–Heinemann, Boston, MA.

McKain, D. L. 1992 Fluidized beds: local heat transfer and slugging behavior. M.Sc. thesis, West Virginia University, Morgantown, WV.

McKain, D. L., Clark, N. N., Karamavruc, A. & Turton, R. 1993 Local time-varying bed-to-tube heat transfer in bubbling fluidized beds. *Proc. of ASME 5th Int. Sym. on Gas–Solid Flows* **166,** 291–299.

McKain, D. L., Clark, N. N., Atkinson, C. & Turton, R. 1994 Correlating local tube surface heat transfer with bubble presence in a fluidized bed. *Powder Technol.* **79,** 69–81.

Mickley, H. S. & Fairbanks, D. F. 1955 Mechanism of heat transfer to fluidized beds. *AIChE Jl* **1,** 372–384.

Mickley, H. S., Fairbanks, D. F. & Hawthorn, R. D. 1961 The relation between the transfer coefficient and thermal fluctuations in fluidized-bed heat transfer. *Chem. Engng Prog. Symp. Ser.* **57,** 51–60.

Saxena, S. C. & Ganzha, V. L. 1984 Heat transfer to immersed surfaces in gas-fluidized beds of large particles and powder characterization. *Powder Technol.* **39,** 199–206.

Saxena, S. C. 1989 *Advances in Heat Transfer*, Vol. 19, pp. 97–190. Academic Press, New York.

Varygin, N. N. & Antonishin, G. M. 1966 *Khim. Mash.* (as cited in Ref. Grewal, N. S. & Saxena, S. C. 1980).

Wen, C. Y. & Yu, Y. H. 1966 A generalized method for predicting the minimum fluidizing velocity. *AIChE Jl* **12,** 610–612.

Werther, J. & Molerus, O. 1973 The local structure of gas fluidized beds—I. A statistically based measuring system. *Int. J. Multiphase Flow* **1,** 103–122.

White, F. M. 1988 *Heat and Mass Transfer*, pp. 134–136. Addison–Wesley, New York.

Zabrodsky, S. S. 1963 *Hydrodynamics and Heat Transfer in Fluidized Beds*. MIT Press, Cambridge, MA.

Zabrodsky, S. S., Antonishin, N. V., Vasiliev, G. M. & Paranas, A. L. 1974 *Vesti Akad. Nauk BSSR. Ser Fiz. Energ. Nauk* **4,** 103 (as cited in Grewal, N. S. & Saxena, S. C. 1980 *Ind. Engng Chem. Proc. Des. Dev.* **20,** 108).